J. Cosmet. Sci., **58**, 359–368 (July/August 2007)

Hair medulla morphology and mechanical properties

RITA WAGNER and INÉS JOEKES, *Departamento de Físico Química, Instituto de Química, Universidade Estadual de Campinas, UNICAMP, CP 6154, 13083-970, Campinas, SP, Brazil.*

Synopsis

The morphology of human hair was extensively discussed in the last century, except for hair medulla, mainly because it was believed to have little or no influence on any useful hair property. Early SEM results showed that medulla is formed by unorganized fibrilar material that could be macrofibrils randomly located in the fiber center. The present paper aims to correlate the fibrilar structures with the macrofibrils using transmission electron microscopy (TEM) and to evaluate the influence of medulla on the mechanical properties of hair.

TEM micrographs show that the interface between cortex and medulla is surrounded by a CMC layer and that there is less electronically dense material between cortical cells. Cortical cells in medulla give the usual microfibril crystalline arrangement. The cells become scarce and less organized in the center of the medulla, which also shows air filled granules.

Average values of the mechanical properties are similar for unmedullated and medullated fibers. However higher dispersion in data for medullated fibers is observed. Unmedulated fibers are more uniform and show smaller diameters. These data indicate that the air cavities in medulla do not interfere with the mechanical properties, but leave hair strength less uniform.

INTRODUCTION

Human hair morphology has been extensively discussed in recent decades due to the interest of the cosmetic industry and the dermatological and forensic sciences (1). With advances in microscopic techniques, it is possible to obtain additional physical and chemical information about morphological hair structures, using atomic force microscopy (AFM) or image mass spectrometry, for example (2,3). Despite more difficult sample preparation methods, the classical electron microscopy techniques (TEM and SEM) are still very much used to study human hair morphology (4,5) mainly because of their resolutions.

Human hair is composed mainly of α-keratin (~ 80% w/w), which is an α-helical protein with high cystine content (6,7). Morphologically, human hair is divided into four units: cortex, cuticle, intercellular material and medulla; the medulla is not always present. The cuticle has an amorphous character. Each cuticle cell is formed by 4 subunits that have distinct chemical compositions and reactivities. Their cross-linked structure depends on the cystine content. (8,9). The cell membrane complex (CMC), which is found between the cuticle cells, is a hydrophilic material rich in polar amino acids and lysine

(2% w/w cystine) (10,11). CMC and endocuticle are believed to be the main diffusion pathways into human hair (12,13).

The cortex is formed by elongated cortical cells surrounded by the CMC. The cortical cell (~100 μm long and 3 μm wide) has an inner fibrillar structure (macrofibrils of 0.4 μm diameter formed by the intermediate filaments of ~10 nm diameter) embedded in a hydrophilic sulphur-rich matrix (12). This well-defined structure gives rise to outstanding mechanical properties (14).

The medulla is located in the centre of the fibre and may be absent, fragmented or continuous (15). It is amorphous and has a high lipid content compared to the rest of the fibre (16). Morphologically, it has been reported that medulla has a porous structure formed by "spongy" keratin (17,18) and some vacuoles filled with air resulting from the differentiation process (17,19). A layer of CMC separates the medulla from the cortex (20). Nevertheless, some authors say that the medulla is just those vacuoles or granules and that the porous structure is formed by an unidentified material (17,20). Medulla represents about 20% of the total fibre section. The effects of this porous structure on mechanical properties are still unknown.

The cuticle subunits were first studied by TEM (21). In TEM, the contrast is created by staining the sliced sample to obtain a two dimensional image. Human hair has to be embedded in a resin to be sliced in an ultramicrotome, otherwise the ultrastructure is not differentiated. In the case of medulla observations, preserving the porous structure and the CMC layer is also difficult. This paper aims to identify the microfibrils in the medulla by TEM and relate their structures to the mechanical properties.

MATERIALS AND METHODS

A one-head tress was observed in a stereoscope and separated into bundles of 40 fibers with or without medulla.

HAIR SAMPLES

A Caucasian dark brown hair sample was obtained from a female donor and separated in medullated and unmedullated fibers using a stereo-microscope. This procedure eliminates chemical and morphological differences by genetics or cosmetic treatments since all fibers come from the same scalp.

TEM OBSERVATIONS

TEM micrographs were obtained in a Philips CM200 microscope, operating at 160 kV. One cm segments of hair fibers were fixed using 2 ml of 2% (v/v) OsO4 (Sigma) in 0.1 mol L^{-1} sodium cacodilate buffer at pH 7, for 4 h in the dark, followed by washing in water or buffer for 30 min. The segments were dehydrated with a series of ethanol solutions of increasing concentration (from 50 to 100%, v/v), for 15 min, two times with each one of the solutions. Then, the hair was exposed twice to a solution of 100% ethanol for 5 min. Spurr resin (standard formulation of low hardening rate, 0.2 g catalyst) used as embedding media, in the following steps: (a) hair segments were placed in closed

flasks filled with resin and ethanol (1:1, v/v) solution, (b) flasks were placed in an acrylic rotor at 3 rpm constant rotation for 4–8 days, (c) the flasks were opened for ethanol evaporation for 24 h, and (d) the hair segments were transferred to proper inclusion molds and cured at 70°C for 24 h. Ultra-thin sections were cut using a Sorvall Porter-Blum Mt2-B ultramicrotome, mounted in a 200 mesh grid and stained with a freshly prepared aqueous solution of 2% uranyl acetate for 15 min and 1% lead citrate for 8 min. Samples were stained just few hours before the observations.

MECHANICAL PROPERTIES

Stress/strain curves were obtained from 40 fibers (5.0 cm length; 24 h conditioning at 25 ± 2°C and 50 ± 5% RH) of each sample using a universal testing machine (EMIC DL 2000) with a 10 N load cell operating at 10 mm/min constant speed. The diameter of each fiber was measured after conditioning using a micrometer (Mitutoyo Ltd.).

RESULTS AND DISCUSSION

MEDULLA MORPHOLOGY BY TEM

Figure 1 shows a representative micrograph of medulla using TEM. It is possible to observe a porous structure composed of cortical cells and air filled vacuoles. (21) The cortical cells are deformed or elongated, showing that they are distributed randomly throughout the medulla. The vacuoles are connected to these cells by peptide bonds derived from citrulline residues, according to Clément *et al.* (22). There are some cavities

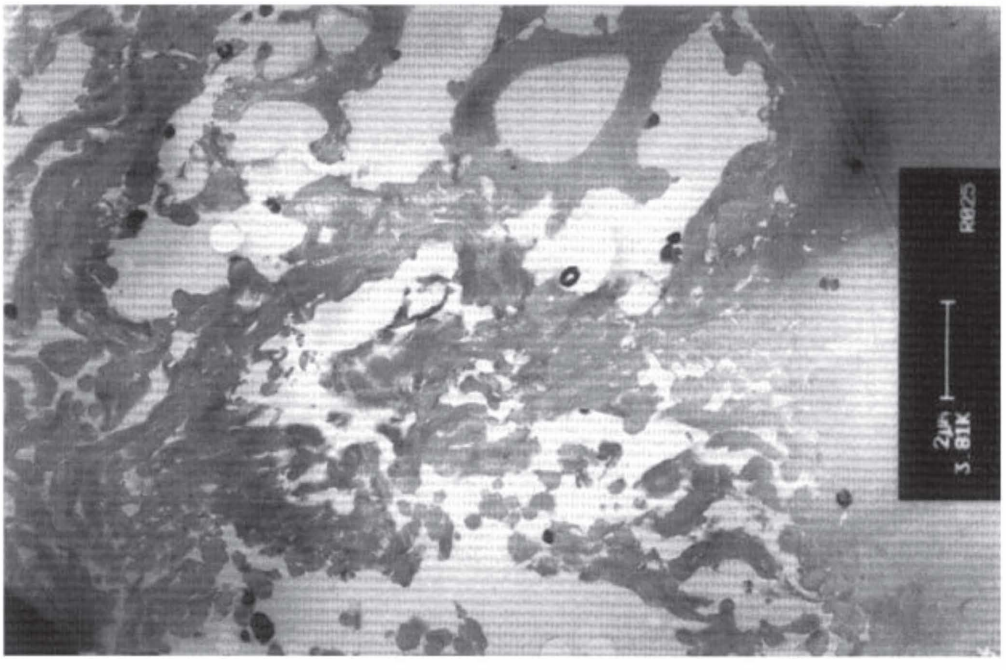

Figure 1. TEM micrograph of human hair medulla.

measuring about (2.8 × 2) μm and a few melanin granules. Also, holes made by the electron beam in the resin film show that these cavities belong to the structure of the medulla and are not artifacts by themselves. Some authors say that the medulla is in fact composed only of the vacuoles. However, as we observed vacuoles mixed with fibril structures (cortical cells) in all the samples, we consider that all of them are part of the structure of the medulla.

Another interesting morphological aspect is the interface between cortex and medulla, shown in Figure 2. The interface is limited by a layer of CMC and empty spaces. The cortical cells become sparse and deformed. Figure 3 shows the microfibril pattern in the medulla/córtex interface (23). This micrograph shows the crystalline character of some cell material in the medulla. Figure 4 shows some microfibrils oriented parallel to the sectioned area, which indicates that cortical cells are randomly distributed.

MECHANICAL PROPERTIES

Typical stress-strain curves of unmedullated or medullated fibers are shown in Figure 5 and 6, respectively. The three main regions of a typical stress-strain curve of human hair, namely the elastic, yield and post-yield regions, are clearly identified. The initial elastic region extends roughly up to 2.5–4% strain. Here the load is taken by the hydrogen bonds establishing the alpha-helical microfibrils along with the matrix. As the hair is stretched to the yield region, the α-helices gradually transform into β-sheets and hair is no longer perfectly elastic (the transformation is complete at about 30% strain and the sheet structure itself exhibits some elasticity). The final phase of the stress-strain curve is the post-yield region where extended microfibrils take the entire load imposed on the hair before leading to complete fracture (24). This is the reason for the slope of the post-yield region being higher than the yield region.

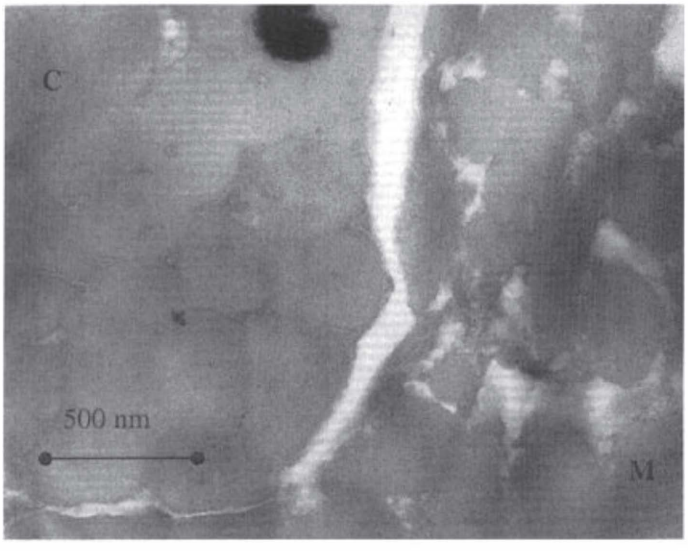

Figure 2. TEM micrograph cortex (C)/ medulla (M) interface.

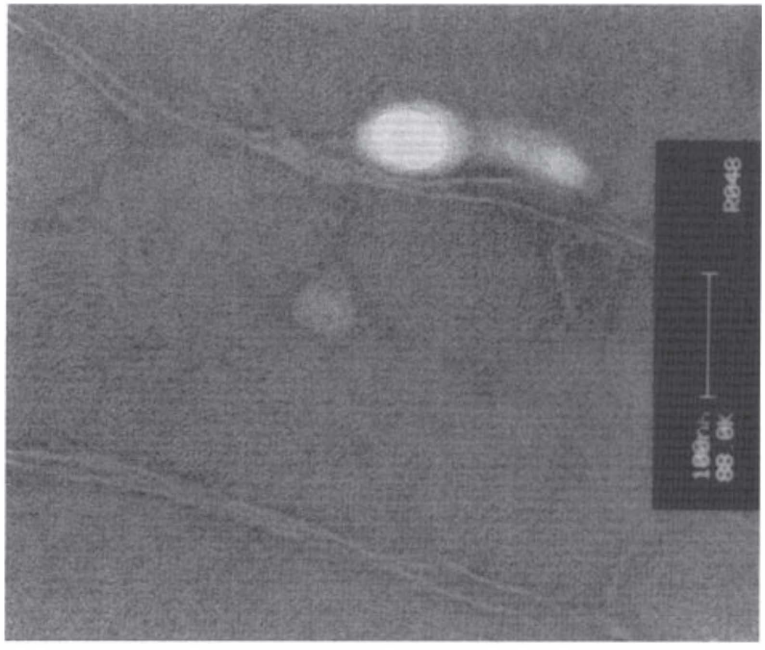

Figure 3. TEM micrograph of microfibrils in medulla transversally oriented to he section.

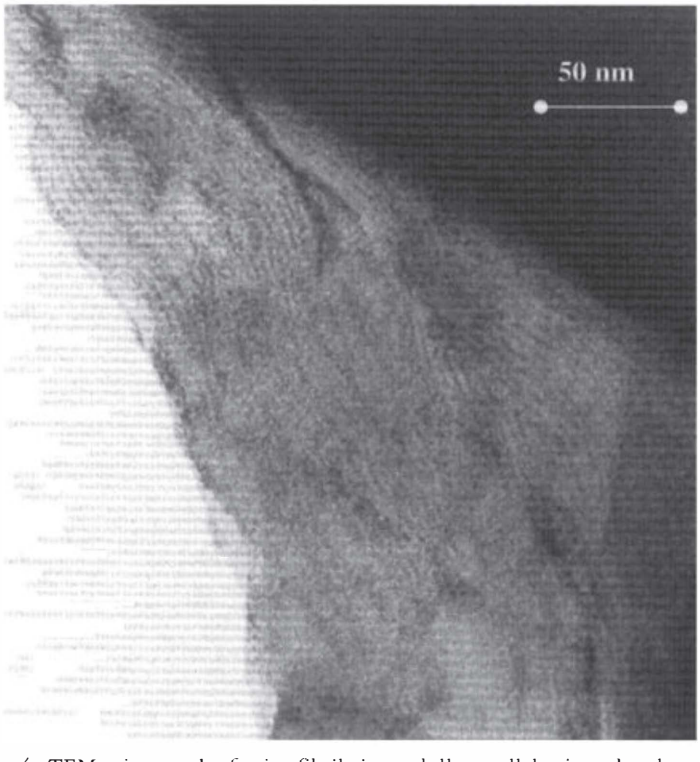

Figure 4. TEM micrograph of microfibrils in medulla parallel oriented to he section.

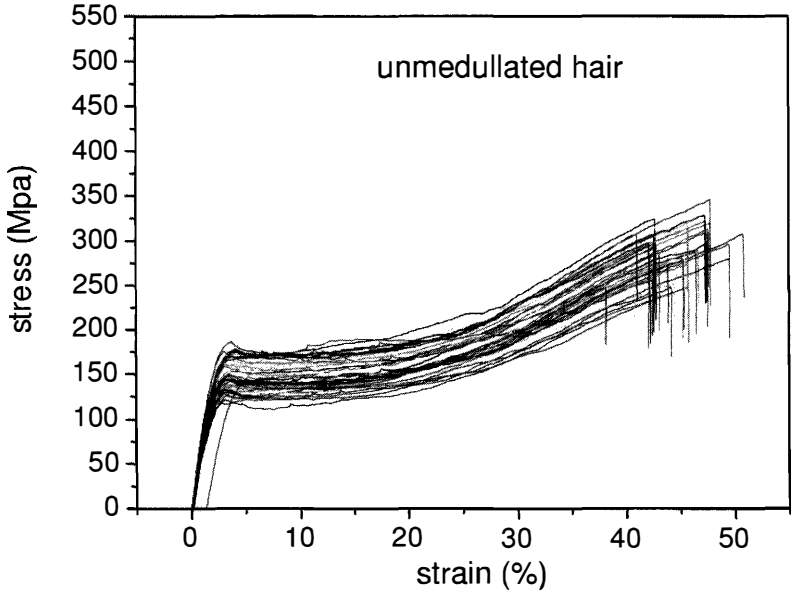

Figure 5. Stress-strain curves of 40 fibers of unmedullated hair.

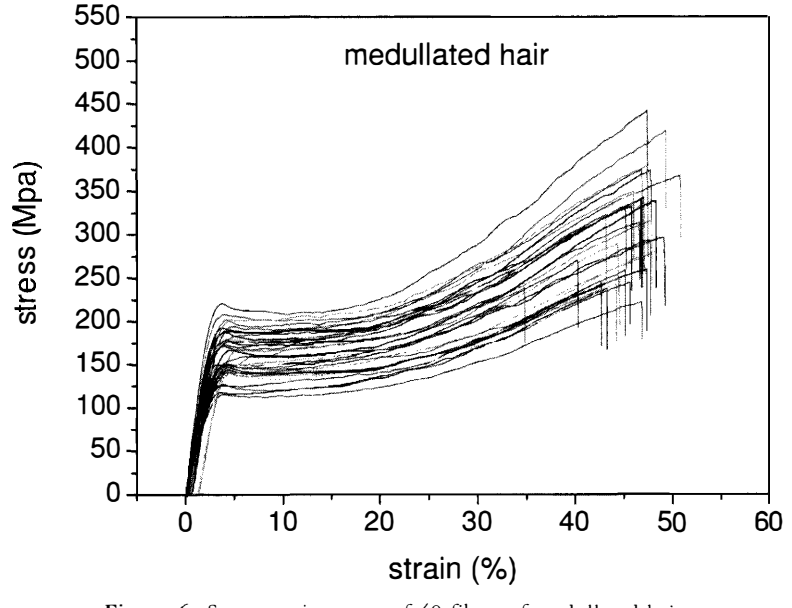

Figure 6. Stress-strain curves of 40 fibers of medullated hair.

A series zone model has been proposed (25) to explain the behavior of hair in the yield and post-yield region. According to the series zone model, hair can be assumed to consist of two alternating zones along the microfibrils, namely the X zone and the Y zone. 30% of the α-helices in the keratin are capable of exhibiting a reversible folding-unfolding nature without breaking the disulfide bonds and these form the X zone, which charac-

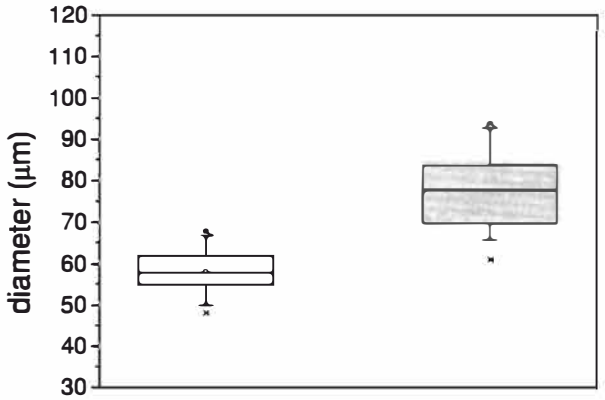

Figure 7. Diameters data for unmedullated (white box) and medullated hair (gray box). Box plots were obtained from 40 hair fiber measurements from each sample.

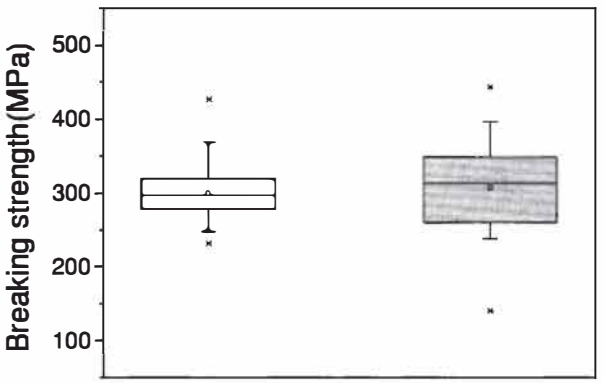

Figure 8. Breaking strength data for unmedullated (white box) and medullated hair (gray box). Box plots were obtained from 40 hair fiber measurements from each sample.

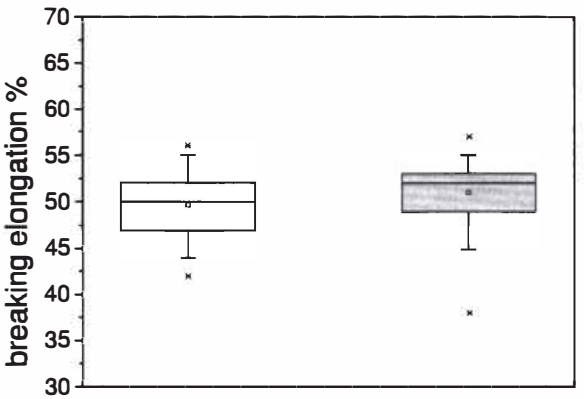

Figure 9. Breaking elongation data for unmedullated (white box) and medullated hair (gray box). Box plots were obtained from 40 hair fiber measurements from each sample.

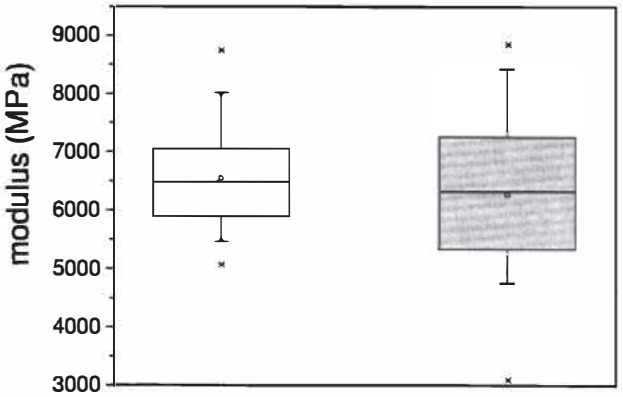

Figure 10. Modulus data for unmedullated (white box) and medullated hair (gray box). Box plots were obtained from 40 hair fiber measurements from each sample.

terizes the yield region. Once the post-yield region is reached, the remaining 70% of the α-helices unfold irreversibly by a compulsory breakdown of the disulphide bonds and they constitute the Y zone. The series zone concept was modified (26) with an extended two phase model to explain the increase of stress in the post-yield region. This model suggests that the increased stress is produced by globular matrix proteins jamming the microfibrils as the fiber is extended into the post-yield region. In this model, water molecules are supposed to be ejected from the matrix at high stress levels, which leads to matrix protein compression between the microfibrils (14). In Chapman's model (27) matrix proteins are supposed to be covalently bonded to fundamental repeat units aligned along the microfibril. The stress-strain curve of the fiber reflects the permanent interaction between microfibril and matrix.

Considering TEM observations for medulla, there are several reasons for expecting different mechanical behavior for medullated hairs. First, the microfibrils are randomly distributed through a 20% of the diameter of the fiber. Thus, most of them are not aligned in the axial direction and this could affect the yield region. According to Clement *et al.* (22), the structures in medulla are cross-linked by peptide bonds from citrulline residues. They might not have the same tensile resistance as the disulfide bonds of the matrix. But when the data is displayed in box plots (Figures 7–10) it is noted that average values are the similar for medullated and unmedullated hair in most cases but that medullated hair shows broader distributions.

Considering the data of Figure 7, unmedullated hair has about 57 μm of diameter or "pure cortex". On the other hand, medullated hair has about 78 μm of diameter but has a porous inner structure of about 15 μm. Deducting the diameter of medulla, medullated hair has about 63 μm of diameter of "pure cortex". This means that both types of hair should show similar mechanical behaviors. The higher variance in stress-strain curves of medullated hair could be caused by the difference between the fiber diameter minus the medulla diameter. Also, the cavities in the medulla structure as mechanical defects generating cracks which lead to ultimate failure.

CONCLUSIONS

TEM micrographs allowed the observation of cortical cells disposed randomly in the medulla. The main evidence was the observation of microfibrils.

Porous medulla leaves hair less uniform leading to broader distributions of tensile mechanical properties. The cavities of the medulla could act as defects which affect the mechanical properties but do not interfere in the crystalline character of the fiber.

ACKNOWLEDGMENTS

The authors acknowledge financial support of FAPESP (Fundação de Amparo à Pesquisa do Estado de São Paulo, Grant 04/13066-0) and of CNPq (Conselho Nacional de Pesquisa, Grant 471061/2004-2). RDCW acknowledges a FAPESP fellowship (Grant 03/13436-0).

REFERENCES

(1) J. R. Smith, A quantitative method for analyzing AFM images of the outer surfaces of human hair, *J. Microsc.,* **191,** 223–228 (1998).
(2) J. A. Swift and J. R. Smith, Atomic force microscopy of human hair, *Scanning,* **22,** 310–318 (2000).
(3) P. Hallégot, R. Peteranderl, and C. Lechene, *In-situ* imaging mass spectrometry analysis of melanin granules in the human hair shaft, *J. Invest. Dermatol,* **122,** 381–386 (2004).
(4) J. R. Smith and J. A. Swift, Maple syrup urine disease hair reveals the importance of 18-methyleicosanoic acid in cuticular delamination, *Micron,* **36**(3), 261–266 (2005).
(5) I. M. Kempson, W. M. Skinner, and P. K. Kirkbride, Calcium distributions in human hair by TOF-SIMS, *Biochim. Biophys. Acta,* **1624,** 1–5 (2003).
(6) L. N. Jones, M. Simon, N. R. Watts, F. P. Booy, A. C. Steven and D. A. D. Parry, Intermediate filament structure: hard α-keratin, *Biophys. Chem.,* **68,** 83–93 (1997).
(7) S. Naito, K. Arai, M. Hirano, N. Nagasawa, and M. J. Sakamoto, Crosslinking structure of keratin. V. Number and type of crosslinks in microstructures of untreated and potassium cyanide treated human hair, *Appl. Polym. Sci.,* **61,** 1913–1925 (1996).
(8) S. Naito and K. Arai, Type and location of SS linkages in human hair and their relation to fiber properties in water, *J. Appl. Polym. Sci.,* **61,** 1918–2113 (1996).
(9) J. R. Smith and J. A. Swift, Lamellar subcomponents of the cuticular cell membrane complex of mammalian keratin fibres show friction and hardness contrast by AFM, *J. Microsc.,* **206,** 182–193 (2002).
(10) K. Röper, J. Föhles, D. Peters, and H. Zahn, Morfological composition of the cuticle from chemically treated wool. 1. Calculating endocuticle content in isolated cuticle from results of amino-acid analysis, *Text. Res. J.,* **54,** 139–143 (1984).
(11) E. G. Bendit and M. Feughelman (Eds.), "Keratin," *Encyclopedia of Polymer Science and Technology, 8th Ed.,* Chapter 1 (1967).
(12) A. Kelch, S. Wessel, T. Will, R. Hintze, R. Wepf, and R. Wiesendanger, Penetration pathways of fluorescent dyes in human hair fibres investigated by scanning near-field optical microscopy, *J. Microsc.,* **200**(3), 179–186 (2000).
(13) L. Pöetsh and M. R. Moeller, On pathways for small molecules into and out of human hair fibers, *J. Forensic Sci.,* **41**(1), 121–125 (1996).
(14) L. Kreplak, A. Franbourg, F. Briki, F. Leroy, D. Dallé J., and Doucet, A new deformation model of hard alpha-keratin fibers at the nanometer sacale: implications for hard alpha-keratin intermediate filament mechanical properties, *Biophys. J.,* **82,** 2265–2274 (2002).
(15) D. W. Deedrick, Microscopy of Hair Part 1: A Practical Guide and Manual for Human Hairs, *Forensic Sci. Commun.,* 1(6) (2004).
(16) L. Kreplak, F. Briki, Y. Duvault, J. Doucet, C. Merigoux, F. Leroy, L. Lèvêque, L. Miller, G. L. Carr, G. P. Williams, and P. Dumas, Profiling lipids across Caucasian and Afro-American hair transverse cuts, using synchroton infrared microspectrometry, *Int. J. Cosmet. Sci.,* **23,** 369–374 (2001).
(17) G. Mahrle and C. E. Orfanos, The spongious keratin and the medulla of human scalp hair, *Arch. Derm. Res.,* **241,** 305–316 (1971).
(18) S. Nagase, S. Shibuichi, K. Ando, E. Kariya, and N. Satoh, Influence of internal structures of hair fiber

on hair appearance. I. Light scattering from the porous structure of the medulla of human hair, *J. Cosmet. Sci.,* **53**(2), 89–100 (2002).
(19) H. Zahn, P. Jolles, and H. Höcker, *Formation and Structure of Human Hair* (Birkhäuser Verlag, Basel, Switzerland), pp. 59, 148 (1997).
(20) J. A. Swift, *Fundamentals of Human Hair Science* (Micelle Press, Weymouth, Dorset), pp. 57 (1997).
(21) M. S. C. Birbeck and E. Mercer, The electron microscopy of the human hair follicle. The hair cuticle, *J. Biophys. Biochem. Cytol.* **3,** 223–233 (1957).
(22) J. L. Clément, A. Le Pareux, and P. F. Ceccaldi, Contribution a l'etude de la medulla des poils, *Ann. Dermatolog. Venereoly,* **108,** 849–857 (1981).
(23) Rogers, G. E., Electron microscope studies of hair and wool, *Ann. New York Acad. Sci.,* **83,** 378–399 (1959).
(24) S. M. Thozhur, A. D. Crocombe, and P. A. Smith, Structural characteristics and mechanical behaviour of beard hair, *J. Mater. Sci.,* 41, 1109–1121 (2006).
(25) Feughelman, M., A two-phase structure for keratin fibers, *Text. Res. J.,* **29,** 223 (1959).
(26) M. Feughelman, A model for the mechanical properties of the alpha-keratin cortex, *Text. Res. J.,* 64, 236–239 (1994).
(27) B. M. Chapman, A mechanical model for wool and other keratin fibers, *Text. Res. J.,* 1102–1109 (1969).